RSC Advances

PAPER

View Article Online
View Journal | View Issue

Cite this: *RSC Adv.*, 2024, **14**, 21241

$CoS_{1.097}$ nanocrystals as new nanoplatforms for photothermal therapy of arterial inflammation†

Ran Lu,[a] Zaiman Ge, *[b] Zeyu Guan,[a] Yong Sun,[ab] Xiaogao Wang[a] and Bing Liu *[c]

Received 31st May 2024
Accepted 28th June 2024

DOI: 10.1039/d4ra04006f

rsc.li/rsc-advances

Cardiovascular diseases caused by atherosclerosis (AS) seriously damage human health. Nano-photothermal technology has been proven to inhibit the development of vascular inflammation by inhibiting the proliferation of inflammatory macrophages. However, photothermal therapy can inhibit the enrichment of AS macrophages in the early stage, but the inhibitory effect is insufficient in the later stage. Herein, we designed and prepared $CoS_{1.097}$ nanocrystals by a simple hydrothermal method as new nanoplatforms for efficient photothermal therapy of arterial inflammation. $CoS_{1.097}$ nanocrystals exhibited the degradability to release the cobalt ions, and can inhibit the proliferation of macrophages both *in vitro* and *in vivo* resulting from the slowly released cobalt ions. Moreover, $CoS_{1.097}$ nanocrystals showed intense absorption in the NIR region, thus showing excellent photothermal performance. When irradiated by an 808 nm laser, the photothermal effect of $CoS_{1.097}$ nanocrystals can more efficiently kill the macrophages which play an important role in the development of atherosclerosis. As far as we know, this is the first work on $CoS_{1.097}$ nanocrystals for photothermal therapy of arterial inflammation.

Introduction

Cardiovascular diseases caused by atherosclerosis (AS) have a serious impact on human health, and its disability rate or mortality rate is increasing. The current treatment methods have problems.[1,2] AS is a chronic inflammatory disease of the arterial wall that leads to luminal stenosis and occlusion; pathological manifestations include endothelial cell dysfunction, platelet adhesion and aggregation, macrophage cell enrichment/foam cell formation, smooth muscle cell migration and proliferation. The phagocytosis of lipids and the release of a large amount of inflammatory factors interact with the vascular wall, which is an important mechanism for macrophages to regulate the inflammatory response of the vascular wall and the formation of atherosclerotic plaques. It has been demonstrated that macrophages play an important role in the formation, development, and instability of arterial plaques, promoting their apoptosis and inhibiting plaque progression.[3,4] In addition, the main clinical methods for treating AS are balloon dilation and stent implantation, which can alleviate ischemic symptoms but also activate macrophages to further exacerbate vascular wall inflammation and promote pathological remodeling of the arterial wall. [5,6] Therefore, inhibiting the activation, infiltration, and proliferation of macrophages and promoting their apoptosis may be an effective way of inhibiting or reversing AS plaque, providing new theoretical basis for the prevention and treatment of AS, which is of great significance.

With the development of nanotechnology, photothermal therapy (PTT) technology, as a minimally invasive technique, brings hope for the treatment of AS.[7–10] Photothermal therapy technology utilizes photothermal conversion materials with near-infrared (NIR) absorption under laser irradiation to achieve local high-temperature damage to cell tissue structures, effectively inhibiting cell proliferation or killing cells at the lesion site.[11,12] The NIR laser with a wavelength range of 700–1400 nm has strong penetration ability into biological tissues, and the attenuation of light during penetration is also very small. It is an important light source widely used in the field of photothermal therapy.[13] At present, there are various types of reported photothermal conversion materials, which can be mainly classified into four categories: precious metals, organic compounds, carbon materials, and semiconductor photothermal conversion materials.[14] Semiconductor photothermal agents show several advantages, such as low price, simple synthesis, easy functionalization, stable photothermal performance, and high absorption coefficient. [15] In recent years, several semiconductor photothermal agents have been used for AS photothermal therapy, including $CuCo_2S_4$ nanomaterials and MoO_2 nanoflowers.[7,8] We also developed Cu_3BiS_3 nanocrystals as an efficient CT contrast agent to monitor carotid inflammation for imaging guided photothermal therapy of

[a]*Department of Vascular Surgery, The First Affiliated Hospital of Bengbu Medical University, Bengbu 233004, Anhui, China*

[b]*Department of General Surgery, Baoshan People's Hospital, Baoshan 678000, Yunnan, China. E-mail: GZM15887672801@163.com*

[c]*Department of Vascular Surgery, The Affiliated Hospital of Qingdao University, Qingdao 266000, Shandong, China. E-mail: qyfyliubing@163.com*

† Electronic supplementary information (ESI) available. See DOI: https://doi.org/10.1039/d4ra04006f

arterial inflammation.[16] Under the combined action of Cu_3BiS_3 nanocrystals and near-infrared lasers, we significantly reduced the number of macrophages during arterial wall remodeling, suppressed wall inflammation, and achieved the goal of preventing wall restenosis. However, photothermal therapy can significantly inhibit the enrichment of AS macrophages in the early stage, but the inhibitory effect is insufficient in the later stage. Therefore, further optimizing the long-term efficacy of this treatment method is of great significance.

Copper based sulfur compounds as photothermal agents can be slowly degraded *in vivo*, mainly because the redox reactions of mixed valence state of copper ions.[17,18] It has been reported that copper ions can be engulfed by macrophages and undergo cell apoptosis *in vitro* and *in vivo* due to the redox reactions leading to the inactivation of the macrophages.[19,20] Cobalt in cobalt sulfur compounds has been reported to exist in mixed valence states, which may have the properties of degradation and photothermal effect. [15] In this work, we designed and prepared $CoS_{1.097}$ nanocrystals by a simple hydrothermal method. $CoS_{1.097}$ nanocrystals can be slowly degraded to release the cobalt ions, and showed intense absorption in the NIR region, thus exhibited excellent photothermal performance. $CoS_{1.097}$ nanocrystals alone can inhibit the proliferation of macrophages both *in vitro* and *in vivo*. When irradiated by an 808 nm laser, the photothermal effect of $CoS_{1.097}$ nanocrystals can more efficiently kill the macrophages which plays an important role in the development of atherosclerosis, thus can be used as an effective way to inhibit the occurrence of hypertension. As far as we know, this is first work on $CoS_{1.097}$ nanocrystals for photothermal therapy of arterial inflammation.

Materials and methods

Synthesis of $CoS_{1.097}$ nanocrystals

$Co(NO_3)_2$ (1 mmol), sodium dimethyldithiocarbamate (2 mmol) and polyvinylpyrrolidone (PVP, 100 mg) were fully dissolved in deionized water (40 mL) under stirring, ethylenediamine (100 μL) was then added. The precursor solution was then transferred to a PTFE hydrothermal reactor, and kept at 180 °C for 24 hours. Black products could be obtained by centrifuge. The products were washed with ethanol and deionized water three times.

Characterization

Transmission electron microscope (TEM) was used to detect the shape and size of $CoS_{1.097}$ nanocrystals. UV-vis spectrophotometer was used to detect the absorption spectrum of $CoS_{1.097}$ nanocrystals. X-ray photoelectron spectrometer (XPS) was used to analyze the electronic spectrum of $CoS_{1.097}$ nanocrystals. X-ray diffractometer (XRD) was used to detect the phase of $CoS_{1.097}$ nanocrystals. Inductively coupled plasma emission spectrometer was used to test the concentration of released ions. 808 nm lasers were used as the light source.

Cell culture

Cells were routinely digested and centrifuged. After removing the supernatant, DMEM high glucose complete medium was added to resuspend the cells. The resuspended cells were incubated in a Petri dish at a density of 1×10^5 cm^{-2} and continue culturing in an incubator (37 °C, 5% CO_2). The cells were digested with trypsin, and continued to expand when the degree of cell fusion reaches 80%.

CCK-8 cell viability test

Raw264.7 cells and Human Umbilical Vein Endothelial Cells (HUVECs) were incubated in a 96-well plate, respectively. After the cell fusion reached 80%, cells were incubated for 24 h with $CoS_{1.097}$ nanocrystals with different concentrations (0, 10, 20, 40, 80, 160 μg mL^{-1}). Then the Raw264.7 cells were excited by an 808 nm laser (0.4 W cm^{-2}, 5 min). Then the medium was removed and the cells were washed with PBS three times to prepare CCK-8 working solution (the ratio of CCK-8 reagent to medium is 1 : 10). After that, CCK-8 working solution (100 μL) was added to each well. After 1 h, a multi-functional microplate reader was used to detect the absorbance at 450 nm wavelength, and the analysis data was collected.

Live/dead cell staining

The cultured Raw264.7 cells were collected and inoculated in a 96-well plate and in an incubator (37 °C, 5% CO_2). When the degree of cell fusion reached 80%, the cells were incubated with or without $CoS_{1.097}$ nanocrystals in high glucose medium for 12 hours. The cells were divided into different groups: PBS or $CoS_{1.097}$ nanocrystals combined with or without an 808 nm laser at a power density of 0.4 W cm^{-2}. After the treatments, the culture supernatant was removed, washed with PBS for three times. CalceinAM and PI were then added, and incubated in a 37 °C incubator for 20 min. Then the cells were observed under an inverted fluorescence microscope.

Animal model construction

All animal experiments were approved by the Animal Ethics Committee of The First Affiliated Hospital of Bengbu Medical University. 28 of 8 weeks-old ApoE−/− mice were selected and fixed on the rat board after anesthetized with chloral hydrate. The left carotid artery was exposed under the microscope *via* making a longitudinal incision in the left neck. A 5 mm length silicone tube was placed around the left carotid artery to wrap it around the left carotid artery. The silk thread was ligated and fixed, and the skin and subcutaneous layers were sutured layer by layer, placed in a 35 °C incubator to wake up, and then put back into the cage.

Photothermal therapy *in vivo*

Two weeks after the surgery, ApoE−/− mice were divided into four groups. The mice were locally injected with PBS or $CoS_{1.097}$ nanocrystals with or without the irradiation of an 808 nm lasers (0.4 W cm^{-2}, 5 min). An infrared thermal imaging camera was used to detect the temperature change of the mice during the treatment.

Histological analysis

The overall status of the mice in each group was observed after surgery. The mice were sacrificed by spinal dislocation on 14 days of photothermal treatment. The left carotid artery and main organs of each group were surgically obtained and dehydrated with 10% sucrose for 1.5–2 h. After that, they are transferred to 30% sucrose for soaking overnight, and then embed frozen sections with OCT to make continuous sections with a thickness of 6–8 μm. The slices were dried overnight in a dark and ventilated place. The next day, the slices were loaded into a slice box and sealed and stored in a −20 °C refrigerator; or after dehydration, they were embedded into paraffin blocks to make continuous slices with a thickness of 6–8 μm. When necessary, the sections were stained for immunofluorescence or immunohistochemical, observed under a fluorescence microscope.

Carotid tissue immunofluorescence staining

Carotid artery slices were soaked in PBS for 3 times (5 min each time) to remove OCT embedding agent. The membrane was perforated with 0.1% Triton-X for 10 min, rinsed with PBS for 3 times. 5% goat serum was blocked at room temperature for 30 min. Diluted anti-mouse CD68 and CD31 antibodies were added, respectively. The slides were removed the next day and rinsed with PBS for 3 times. DAPI (1 : 500) was added dropwise to stain nuclei for 30 s, rinsed twice with PBS for 5 min each time. After anti-fluorescence quenching, the tablet was sealed, observed and photographed under a fluorescence microscope.

Carotid artery hematoxylin-eosin staining

The slices of carotid artery and main organ tissues were rinsed with distilled water for 3 times, 5 minutes each time. Then the slices were stained with hematoxylin and eosin (HE) dye for 2 minutes, rinsed with distilled water. The slices were gradually dehydrated with 70%, 85%, 95% and 100% alcohol in sequence. Finally, the slices were observed under microscope after sealing with neutral gum.

Results and discussion

Hydrophilic $CoS_{1.097}$ nanocrystals were synthesized by hydrothermal method in the presence of poly vinyl pyrrolidone (PVP). Thus, $CoS_{1.097}$ nanocrystals are hydrophilic and coated by PVP, evidenced by Fourier transform infrared spectrum (FTIR, Fig. S1†). To confirm the crystallographic structure, the nanocrystals were first measured by powder X-ray diffraction (XRD). As shown in Fig. 1A, all the XRD peaks of the nanocrystals can be well indexed as $CoS_{1.097}$ nanocrystals (JCPDS No. 19-0366) with no detected peaks of any other phases. The perfect match indicated that the synthesized $CoS_{1.097}$ nanocrystals with high crystallinity and high purity. More information on the

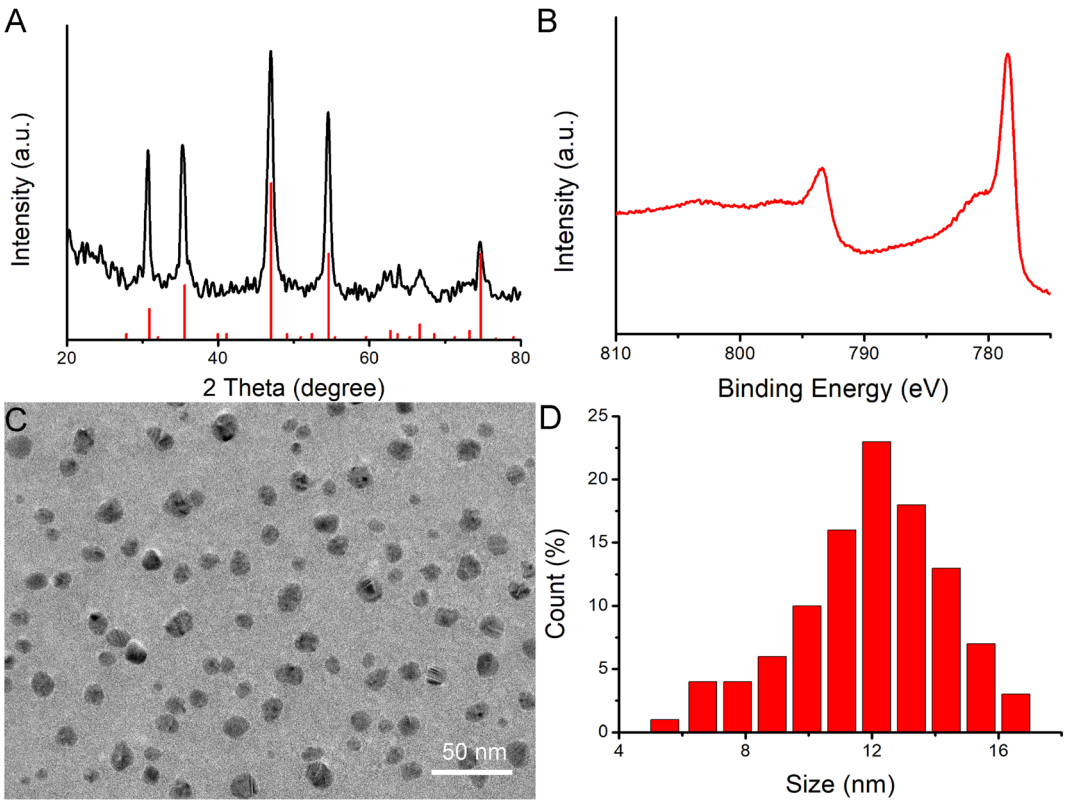

Fig. 1 (A) Powder XRD patterns of the as-prepared nanocrystals (black line) and the standard (red line) $CoS_{1.097}$ nanocrystals from the JCPDS card (No. 19-0366). (B) High resolution XPS spectra of Co 2p in the as-prepared $CoS_{1.097}$ nanocrystals. (C) TEM image of $CoS_{1.097}$ nanocrystals. (D) Size histograms represent the dimension distribution of the $CoS_{1.097}$ nanocrystals.

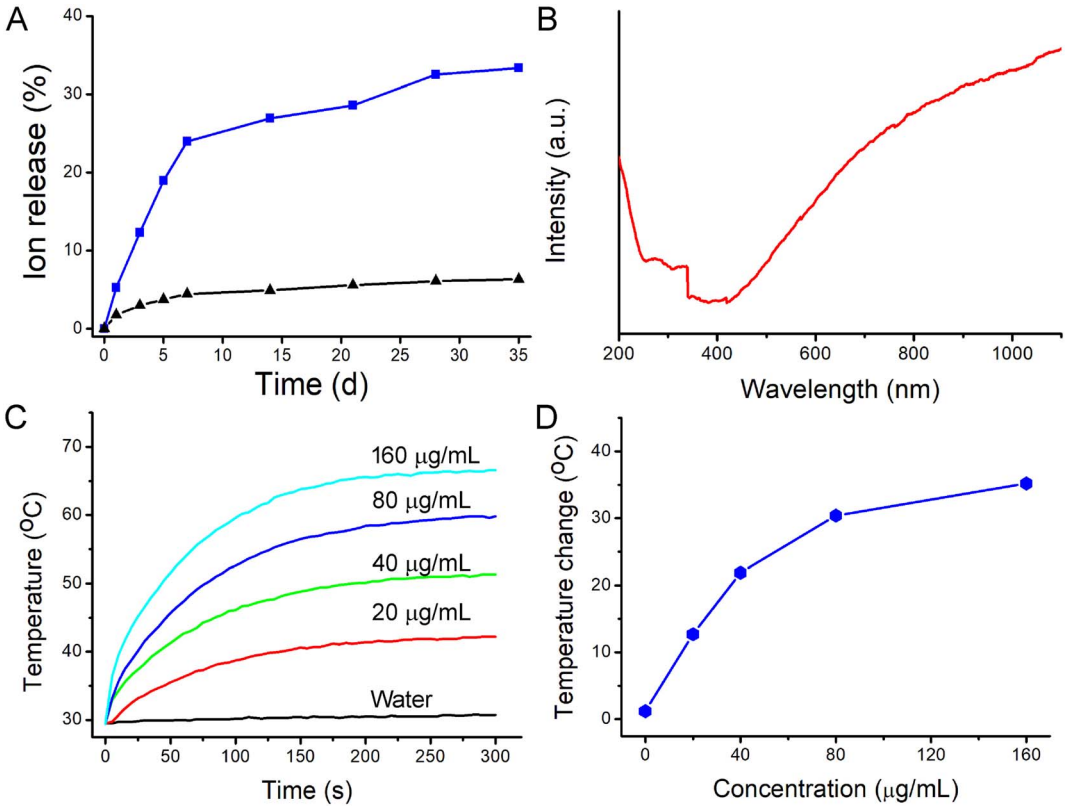

Fig. 2 (A) Accumulated release profiles of Co ion from $CoS_{1.097}$ nanocrystals in PBS (pH = 5.4, blue line) and water (black line). (B) UV-vis absorbance spectrum for the aqueous dispersion of $CoS_{1.097}$ nanocrystals. (C) Temperature of $CoS_{1.097}$ nanocrystals with different concentrations (0, 20, 40, 80, 160 μm mL^{-1}) under the excitation of an 808 nm laser (0.4 W cm^{-2}, 300 s). (D) Temperature change as a function of the concentration of $CoS_{1.097}$ nanocrystals.

composition and chemical bonding state of the nanocrystals were performed by X-ray photoelectron spectroscopy (XPS, Fig. S2†), showing that the as-prepared sample is mainly composed of Co and S elements without other obvious impurities (the C and O peaks originate from the ligands). Fig. 1B shows high-resolution XPS analysis of Co 2p of $CoS_{1.097}$ nanocrystals. A Co $2p_{3/2}$ (777.8 eV) peak and a Co $2p_{1/2}$ (793.1 eV) peak, as well as two shakeup satellites, in the Co 2p spectrum confirmed the coexistence of two cobalt oxidation state: Co^{2+} and Co^{3+}. [21] The morphology and size of the as-synthesized $CoS_{1.097}$ nanocrystals were measured by transmission electron microscopy (TEM). Shown in Fig. 1C and D, the synthesized $CoS_{1.097}$ nanocrystals showed good dispersion with a size of 12.5 nm, indicating that the synthesized nanocrystals were suitable for bioapplication.

As for the applied mixed valence metal compound biomaterials, they are more easily degraded *in vivo*. There was a coexistence of Co^{2+} and Co^{3+} within $CoS_{1.097}$ nanocrystals (Fig. 1B), we thus examined the release rate of Co from $CoS_{1.097}$ nanocrystals by inductively coupled plasma atomic emission spectroscopy (ICP-AES). The results showed that the percentages of released Cu in PBS (pH = 5.4) at weeks 1 and 5 were 23.89% and 33.28%, respectively; while those in water exhibited almost no changes. The nonequivalent-valency ions lead to ionized free carriers for achieving near-infrared (NIR) absorption. As expected, the as-prepared $CoS_{1.097}$ nanocrystals showed broad and strong absorption in the NIR region with a high molar extinction coefficient of 5.8×10^6 M^{-1} cm^{-1} at 808 nm (Fig. 2B). The intense NIR absorption of $CoS_{1.097}$ nanocrystals motivated us to evaluate the photothermal performance of $CoS_{1.097}$ nanocrystals. The aqueous dispersions of nanocrystals with varied concentrations were placed in the PE tubes, and excited by an 808 nm laser. The temperature change was recorded by infrared thermal imager. As shown in Fig. 2C, the temperature of aqueous dispersions of nanocrystals increased dramatically under the irradiation of the 808 nm laser, while the temperature of pure water showed little change, indicating that $CoS_{1.097}$ nanocrystals exhibited excellent photothermal effect. As the concentration increased, the elevated temperature increased. Obviously, $CoS_{1.097}$ nanocrystals showed concentration-dependent photothermal effect. Fig. 2D provides the direct relationship between the concentration of $CoS_{1.097}$ nanocrystals and the temperature. When the concentration was 40 ppm, the temperature of the aqueous dispersion was increased by 21.9 °C, while the temperature of pure water was increased by less than 2 °C, demonstrating the excellent photothermal performance of $CoS_{1.097}$ nanocrystals. To evaluated the NIR photostability of the $CoS_{1.097}$ nanocrystals, the aqueous dispersion (50 ppm) was irradiated with 808 nm laser (1.0 W cm^{-2}) for 10 min (LASER ON, Fig. S3†), respectively, followed by naturally cooling

to room temperature for 30 min (without irradiation, LASER OFF). It was showed that there was little loss of the maximum temperature elevation after 4 cycles of LASER ON/OFF. The result indicated that the $CoS_{1.097}$ nanocrystals showed good NIR photostability.

The mouse macrophage Raw264.7 cells have been widely utilized to study the function and behavior of macrophages. In order to detect the cytotoxicity of $CoS_{1.097}$ nanocrystals, we used $CoS_{1.097}$ nanocrystals at different concentrations (0–160 μm mL^{-1}) to co-culture with macrophages for 12 h, and then tested the cell activity of each group by CCK-8 experiment. The results showed that the concentration was below 20 ppm, $CoS_{1.097}$ nanocrystals had no significant effect on the activity of macrophages; when the concentration reached from 40 to 160 μm mL^{-1}, the macrophage activity was significantly decreased (Fig. 3A). The optimal treatments of arterial inflammatory diseases should inhibit the activity of inflammatory cells but avoid injury to vascular endothelium; otherwise vascular barrier function is impaired, leading to arterial restenosis. Thus, we evaluated the cytotoxicity of $CoS_{1.097}$ nanocrystals on

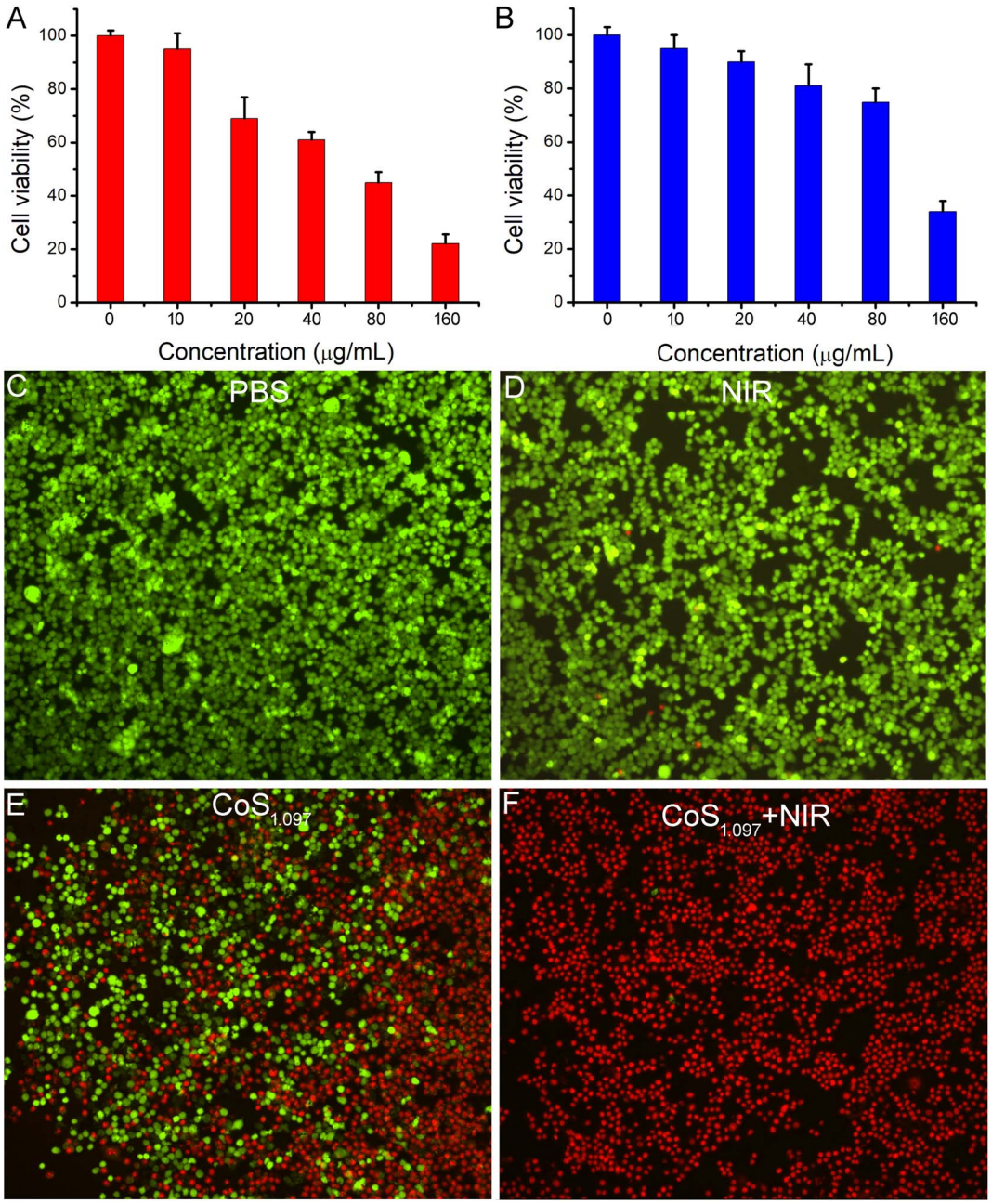

Fig. 3 Relative cell viability of (A) macrophages and (B) HUVECs treated with $CoS_{1.097}$ nanocrystals at different concentrations. Confocal images of fluorescence staining live/dead cells incubated with $CoS_{1.097}$ nanocrystals then exicted with/without an 808 nm laser: (C) PBS, (D) PBS and the 808 nm laser irradiation (0.4 W cm^{-2}), (E) 80 μm mL^{-1} $CoS_{1.097}$ nanocrystals, (F) 80 μm mL^{-1} $CoS_{1.097}$ nanocrystals and the 808 nm laser irradiation. Magnification: 200 times.

and HUVECs (Fig. 3B). Notably, with a concentration of 80 ppm, the viability of HUVECs was almost no unaffected, while that of macrophages was significantly reduced. These results indicated that 40 μm mL^{-1} was the minimum effective dose of $CoS_{1.097}$ nanocrystals. Additionally, based on the photothermal curves of $CoS_{1.097}$ nanocrystals under the action of near-infrared light, $CoS_{1.097}$ nanocrystals showed a good heating effect at a concentration of 40 μm mL^{-1} with the temperature increased by 21.9 °C. We thus chose 40 ppm as the concentration used in subsequent experiments. We also stained the living/dead cells of each treatment group to further clarify the status of the cells in each treatment group. As shown in Fig. 3C–F, no significant cell death was observed in the control group, while nearly 39.5% of the cells treated with 40 μm mL^{-1} $CoS_{1.097}$ nanocrystals were killed, and more than 95.8% of the cells treated with 40 μm mL^{-1} $CoS_{1.097}$ nanocrystals combined with an 808 nm laser (0.4 W cm^{-2}) were killed. These results indicated that the photothermal effect of 40 μm mL^{-1} $CoS_{1.097}$ nanocrystals showed the great potential for the treatment of arterial inflammation and atherosclerosis.

We then further used ApoE−/− mice to make arterial inflammation and stenosis models for photothermal therapy *in vivo*. ApoE−/− mice were divided into two groups: control group and experiment group. The mice were locally injected with PBS or $CoS_{1.097}$ nanocrystals. The mice were simultaneously excited by the 808 nm lasers (0.4 W cm^{-2}, 300 s). The infrared thermal imager dynamically recorded the local temperature changes of the left neck of the mouse. As shown in Fig. S4,† the local temperature of the $CoS_{1.097}$ + PTT group can rapidly increase to 46.1 °C within 300 s, while the local temperature of the PBS group increase by less than 2 °C within 300 s. Therefore, $CoS_{1.097}$ nanocrystals still showed excellent photothermal effect *in vivo* driven by the 808 nm laser.

Two weeks after the treatments *in vivo*, the left carotid artery of each group of mice was removed for immunofluorescence staining. In immunofluorescence, we used CD68 as a marker for macrophages and CD31 as a marker for vascular smooth muscle cells. The results showed that the number of infiltrated $CD68^{+}$ macrophages in the middle artery wall of the control groups (PBS or NIR) was higher than that of $CoS_{1.097}$ nanocrystals group (Fig. 4A–C). What's more, the number of macrophage of the $CoS_{1.097}$ nanocrystals + PTT group was minimal (Fig. 4D and S5†), indicating that the photothermal therapy based on $CoS_{1.097}$ nanocrystals can effectively inhibit the infiltration of macrophages in the inflammatory arterial wall, which may reduce the adverse results caused by the infiltration of a large number of inflammatory macrophages.

In order to further evaluate the effect of ablation of arterial wall macrophages on reducing the thickness of the arterial wall and inhibiting the progress of arterial stenosis, we tested the thickness of the carotid artery wall of mice by HE staining. The results showed that $CoS_{1.097}$ nanocrystals partially decreased the carotid intima-media thickness (Fig. 5A–C). Moreover, the thickness of the intima-media in the $CoS_{1.097}$ nanocrystals +

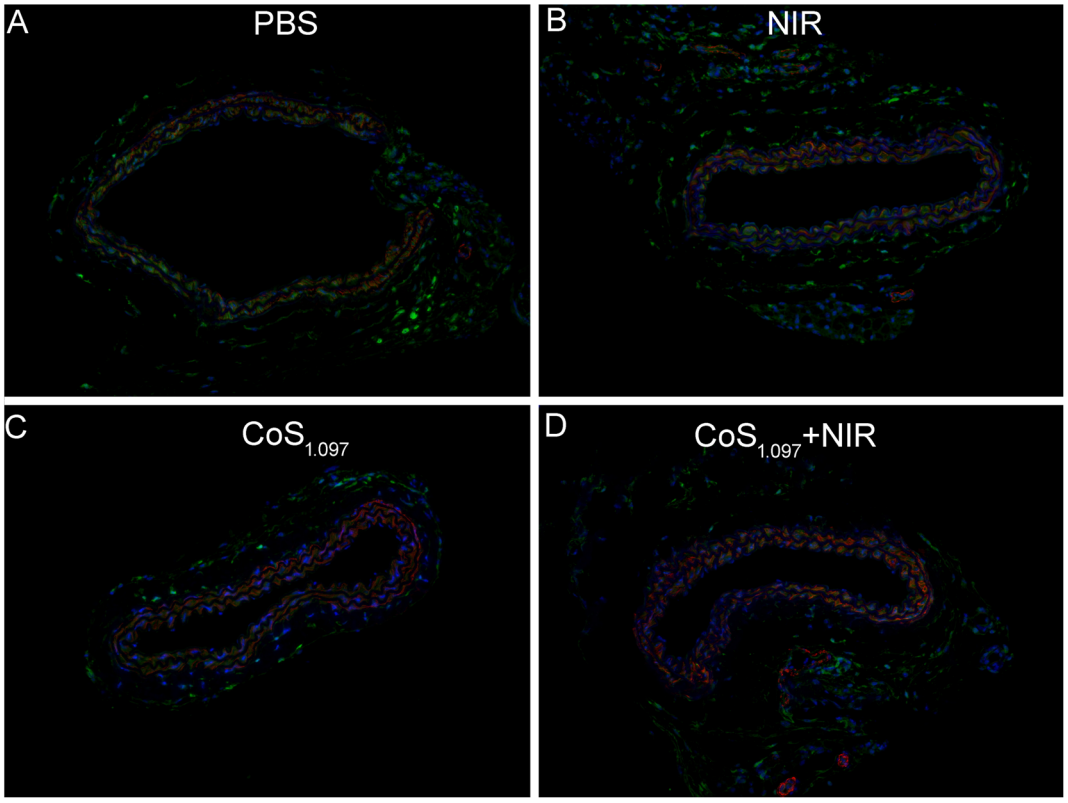

Fig. 4 Representative images of immunofluorescence co-staining in collar-implanted group mice with different treatments: (A) PBS; (B) PBS and NIR laser irradiation; (C) $CoS_{1.097}$ nanocrystals; (D) $CoS_{1.097}$ nanocrystals and NIR laser irradiation. Magnification: 200 times.

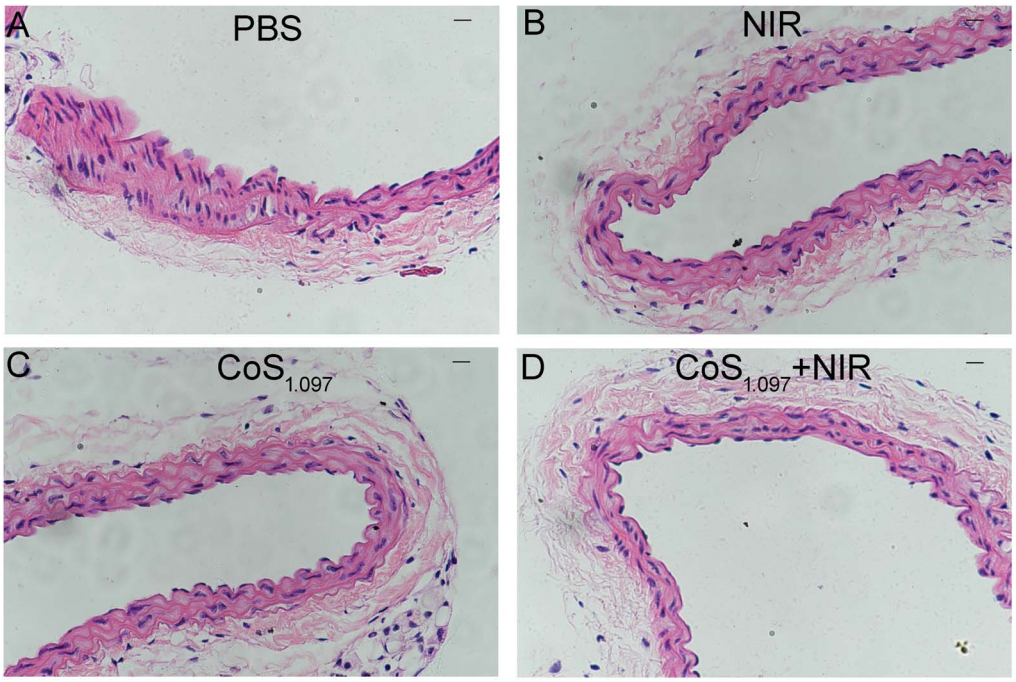

Fig. 5 HE staining of the carotid artery in different groups: (A) PBS, (B) NIR, (C) $CoS_{1.097}$ nanocrystals, (D) $CoS_{1.097}$ nanocrystals + NIR. Magnification: 200 times.

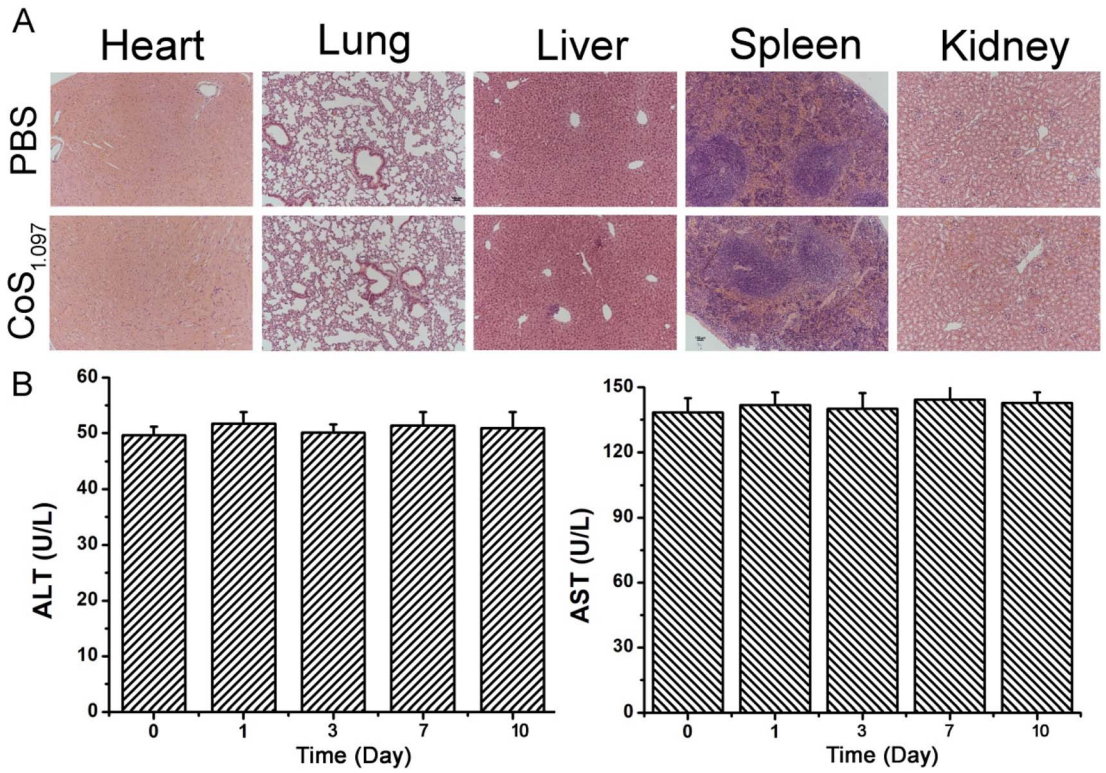

Fig. 6 (A) H&E stained slices of main organs. Magnification: 100 times. (B) Blood biochemistry of mice receiving intravenous injection of $CoS_{1.097}$ nanocrystals at different time points. The examined parameters include aspartate aminotransferase (ALT, left) and alanine aminotransferase (AST, right).

NIR group was much lower than that in the control (PBS/NIR) groups (Fig. 5D). Effectively inhibit the thickening of the intima/media of the arterial wall, thereby reducing the occurrence of arterial stenosis. In addition, this result was consistent with the arterial wall inflammatory macrophage infiltration results (Fig. S6†). The arterial intima-media thickness was positively correlated with the amount of arterial wall macrophage infiltration to a certain extent, further indicating that

inflammatory macrophage infiltration in the artery, the key role in wall hyperplasia. To sum up, photothermal therapy based on $CoS_{1.097}$ nanocrystals can effectively suppress the thickening of the arterial wall by ablating inflammatory macrophages in the arterial wall, thereby effectively inhibiting the occurrence of arterial stenosis.

As *in vivo* biosafety of nanomedicines is always of great concern for application in photothermal therapy, further biosafety experiment on histological examination analysis with H&E staining for the main organs was conducted to observe the size, shape and number of cells after the intravenous injection of $CoS_{1.097}$ nanocrystals (15 mg kg^{-1}). From the HE staining of the major organs, including heart, kidney, spleen, liver and lung, no obvious inflammation or damage is observed (Fig. 6A). The parameters related to the serum biochemistry (Fig. 6B) showed no meaningful changes. We also studied the distribution of the $CoS_{1.097}$ nanocrystals, mice were intravenously injected with the $CoS_{1.097}$ nanocrystals. At different intervals of time (*i.e.*, 1, 3, 7, 10 days, $n = 3$ at each time point), mice were sacrificed to obtain major organs including kidney, spleen, heart, liver, and lung. These organs were digested and solubilized. An ICP-MS analysis was used to determine Co content in each organ. It was (Fig. S7†) found that the $CoS_{1.097}$ nanocrystals mainly accumulate at spleen and liver, indicating that $CoS_{1.097}$ nanocrystals was mainly degraded in these two organs. The evidences confirmed that the $CoS_{1.097}$ nanocrystals have promising potential for photothermal therapy. However, deep systematic studies of pharmacokinetics and pharmacodynamics are still pretty important for future clinical application of such a material.

Conclusions

In conclusion, $CoS_{1.097}$ nanocrystals with a size of about 12.5 nm were successfully designed and prepared by a simple hydrothermal method. $CoS_{1.097}$ nanocrystals can inhibit the proliferation of macrophages both *in vitro* and *in vivo* resulted from the released cobalt ions. When irradiated by an 808 nm laser, the photothermal effect of $CoS_{1.097}$ nanocrystals can more efficiently kill the macrophages which play an important role in the development of atherosclerosis. Therefore, $CoS_{1.097}$ nanocrystals show great potential for photothermal therapy of arterial inflammation.

Ethical statement

All animal procedures were performed in accordance with the Guidelines for Care and Use of Laboratory Animals of The First Affiliated Hospital of Bengbu Medical University and approved by the Animal Ethics Committee of The First Affiliated Hospital of Bengbu Medical University.

Data availability

The data supporting this article have been included in the main article and the ESI.†

Author contributions

Ran Lu: methodology, investigation, visualization, writing – original draft. Zaiman Ge: supervision, writing – review & editing. Zeyu Guan: investigation, visualization, writing – original draft. Yong Sun: visualization, data curation. Xiaogao Wang: investigation, visualization. Bing Liu: supervision, writing – review &editing.

Conflicts of interest

There is no conflict of interest to declare.

Acknowledgements

This study was supported by the Natural Science Research Project of Anhui Educational Committee (2022AH051422).

References

1 G. A. Roth, C. O. Johnson, N. J. Kassebaum, A. H. Mokdad, M. Naghavi and T. Vos, *Circulation*, 2017, **135**, A19.
2 G. C. Death, *Lancet*, 2017, **390**, E38.
3 P. M. Ridker and T. F. Luscher, *Eur. Heart J.*, 2014, **35**, 1782–1791.
4 M. Nahrendorf and F. K. Swirski, *Science*, 2015, **349**, 237–238.
5 T. Yamashita, N. Sasaki, K. Kasahara and K. Hirata, *J. Cardiol.*, 2015, **66**, 1–8.
6 W. F. Fearon and D. T. Fearon, *Circulation*, 2008, **117**, 2577–2579.
7 X. Zhang, J. Liu, X. Yang, G. He, B. Li, J. Qin, P. R. Shearing, D. J. L. Brett, J. Hu and X. Lu, *Nanoscale*, 2019, **11**, 9733–9742.
8 X. Wang, X. Wu, J. Qin, K. Ye, F. Lai, B. Li, G. He, X. Lu, D. J. L. Brett and I. P. Parkin, *ACS Appl. Mater. Interfaces*, 2019, **11**, 41009–41018.
9 W. R. Chen, R. L. Adams, R. Carubelli and R. E. Nordquist, *Cancer Lett.*, 1997, **115**, 25–30.
10 J. Liu, X. Guo, Z. Zhao, B. Li, J. Qin, Z. Peng, G. He, D. J. L. Brett, R. Wang and X. Lu, *Appl. Mater. Today*, 2019, 100457.
11 J. Yang, J. Choi, D. Bang, E. Kim, E. K. Lim, H. Park, J. S. Suh, K. Lee, K. H. Yoo, E. K. Kim, Y. M. Huh and S. Haam, *Angew. Chem., Int. Ed.*, 2011, **50**, 441–444.
12 B. Li, K. Ye, Y. Zhang, J. Qin, R. Zou, K. Xu, X. Huang, Z. Xiao, W. Zhang, X. Lu and J. Hu, *Adv. Mater.*, 2015, **27**, 1339–1345.
13 B. Li, Y. Zhang, R. Zou, Q. Wang, B. Zhang, L. An, F. Yin, Y. Hua and J. Hu, *Dalton Trans.*, 2014, **43**, 6244.
14 Z. Chen, Q. Wang, H. Wang, L. Zhang, G. Song, L. Song, J. Hu, H. Wang, J. Liu, M. Zhu and D. Zhao, *Adv. Mater.*, 2013, **25**, 2095–2100.
15 B. Li, F. Yuan, G. He, X. Han, X. Wang, J. Qin, Z. X. Guo, X. Lu, Q. Wang, I. P. Parkin and C. Wu, *Adv. Funct. Mater.*, 2017, **27**, 1606218.
16 R. Lu, J. Zhu, C. Yu, Z. Nie and Y. Gao, *Front. Bioeng. Biotechnol.*, 2020, **8**, 981.

17 J. Liu, P. Wang, X. Zhang, L. Wang, D. Wang, Z. Gu, J. Tang, M. Guo, M. Cao, H. Zhou, Y. Liu and C. Chen, *ACS Nano*, 2016, **10**, 4587–4598.
18 M. Zhang, X. Liu, Q. Luo, Q. Wang, L. Zhao, G. Deng, R. Ge, L. Zhang, J. Hu and J. Lu, *Chem. Eng. J.*, 2020, **389**, 124450.
19 M. Chen, Y. Luo, J. Xu, M.-X. Chang and J.-X. Liu, *Front. Immunol.*, 2019, **10**, 2599.
20 Z. Wu, Z. Xu, H. Pu, W. Li, J. Liu, Z. Zhao, X. Lu, K. Lin and B. Li, *Appl. Mater. Today*, 2021, **25**, 101214.
21 J. Tang, Y. Ge, J. Shen and M. Ye, *Chem. Commun.*, 2016, **52**, 1509–1512.